DOI: 10.1002/cjoc.201200505

Effect of Vacancy Defects on the Young's Modulus and Fracture Strength of Graphene: A Molecular Dynamics Study

Zhu, Jian(朱剑) He, Ming(贺明) Qiu, Feng*(邱枫)

State Key Laboratory of Molecular Engineering of Polymers, Department of Macromolecular Science, Fudan University, Shanghai 200433, China

The Young's modulus of graphene with various rectangular and circular vacancy defects is investigated by molecular dynamics simulation. By comparing with the results calculated from an effective spring model, it is demonstrated that the Young's modulus of graphene is largely correlated to the size of vacancy defects perpendicular to the stretching direction. And a linear reduction of Young's modulus with the increasing concentration of monoatomic-vacancy defects (*i.e.*, the slope of −0.03) is also observed. The fracture behavior of graphene, including the fracture strength, crack initiation and propagation are then studied by the molecular dynamics simulation, the effective spring model, and the quantized fracture mechanics. The blunting effect of vacancy edges is demonstrated, and the characterized crack tip radius of 4.44 Å is observed.

Keywords graphene, mechanical properties, molecular dynamics simulation, vacancy defect

Introduction

Graphene, consisting of a single layer of carbon atoms arranged in two-dimensional (2D) honeycomb lattices, has been attracting significant attentions due to its intriguing physical properties, for example, the quantum Hall effect at room temperature, ambipolar electric field effect, tunable band gap, high Young's modulus and fracture strength.[1-7] Owing to the thermal fluctuation, 2D single-layer crystals were not supposed to actually exist in a free state at finite temperature.[8] Until the groundbreaking discovery of single-layer graphene (SLG) in 2004,[1,9] it is found that carbon atoms can form long-range, high-quality, and continuous crystals in 2D dimensions, which is ascribed to the strong interatomic bonds in graphene preventing the formation of dislocations or defects even at high temperature, as well as the gentle three-dimensional (3D) crumping of graphene sheet to minimize the total free energy by suppressing thermal vibrations.[10] To date, both pristine and modified graphene have exhibited remarkably high mechanical, electronic, and optical properties, making it become promising candidates in the application of organic electronics, energy storages, mechanical resonators, chemical sensors and so on.[11,12]

The physical properties of graphene with high-perfection crystalline lattices are definitely outstanding. However, structural defects unintentionally generated in the chemical or physical exfoliation processes will heavily deteriorate the performance of graphene-based devices.[13] Although the defect-free pristine graphene prepared by mechanical exfoliation using the 'scotch-tape' method shows exceptional properties,[9] this manual-exfoliation method is not appropriate for large-scale device fabrication. The chemical vapor deposition (CVD)-grown graphene[11] and the chemically-exfoliated graphene[14] both suffer from relatively poor performances due to the existence of a large amount of structural defects. In particular, chemically-exfoliated graphene contains irreversible lattice disorders and vacancy defects, which have been observed by scanning transmission electron microscopy (STEM).[15] As to the CVD-grown graphene, its mechanical properties are largely dominated by the grain boundaries,[16] which have been well studied by combining experiments and atomistic simulations.[17,18] Based on the experimental and theoretical data for carbon nanotubes (CNTs) and graphene, it is concluded that such structural defects may weaken the sp^2-bonds around the defects, reduce the fracture strength, and damage the device durability. Thus efficient methods to minimize or reconstruct vacancy-type defects are needed to eliminate these detrimental effects.[13] In comparison to experiments, simulation methods are good at atomic structure modeling and analysis, which enables us to systematically investigate intrinsic defects, such as vacancies, dislocations, stacking faults and voids. For example, the simulation on vacancy defect and cracks on graphene has revealed that the fracture strength primarily depends on the vacancy cross section perpendicular to the tensile direction and the atomic structure near the fracture initiation

* E-mail: fengqiu@fudan.edu.cn
Received May 24, 2012; accepted July 1, 2012.

point.[19] Using atomistic simulation, researchers have well investigated the Stone-Wales defects on CNTs and graphene, whose formation energy and fracture mechanism have been derived.[20,21] Recently, more simulation works have extended to investigate multi-defect influence, whose concentration and distribution effect have been studied.[22-24]

The fracture behavior of bulk crystals is usually studied by the continuous fracture modeling (CFM) method, wherein the fractures are supposed to continuously pass through bulks. But CFM method is not fit to the fracture behavior of nanostructure materials, because the fracture in nanostructures is dominated by the cracking of single bonds rather than the ideal continuous fractures. In order to appropriately describe the behavior of this non-continuous fracture in nanostructures, a quantized fracture mechanics (QFM) was proposed by Pugno and Ruoff, which is a modified Griffith's theory, suggesting that the fracture strength is mostly related to the crack tip radius and the length of the crack.[25] The fracture strength based on the QFM modeling is given by Eq. (1):

$$\sigma_f(l,\rho)=\sigma_c\sqrt{\frac{1+\rho/2L_0}{1+2l/L_0}} \quad (1)$$

where σ_c is the fracture strength of the defect-free nanostructure, ρ is the crack tip radius, l is the length of the crack, and L_0 is the fracture quantum (*i.e.*, the minimum propagation distance of the crack). According to Eq. (1), for a nanostructure with cracks, its fracture strength increases with the crack tip radius and decreases with the crack length. The fracture strengths of CNT, β-SiC nanorod and α-Si_3N_4 whisker calculated by the QFM modeling are very close to their experimental values.

Herein, we investigate the mechanical properties of graphene with various vacancy defects using the QFM modeling, MD simulation, and an effective spring model. The effects of the shape, the size, and the concentration of vacancy defects on the Young's modulus, fracture strength, and crack initiation behavior are investigated.

Simulation Model

The MD simulation of the fracture behavior of graphene was performed using the program of LAMMPS and the adaptive inter molecular reactive empirical bond order (AIREBO) potential was used to define the force field.[26] Originating from the Tersoff-Brenner potential which allows the simulation of bond breaking and reforming, the AIREBO potential extends to include the intermolecular interactions between non-bonded atoms as well as the torsional interactions associated with a connected sequence of three bonds.[27-29] Brenner and coworkers previously provided the AIREBO parameters for the carbon-hydrogen system, in which the two cutoff distances of the carbon-carbon bonding (*i.e.*, D_1 and D_2) were set as 1.7 Å and 2.0 Å, respectively. However, by using these cutoff distances, graphene exhibits an unphysical ductile behavior during the stretching process, attributed to the discontinuous second derivative of the potential between D_1 and D_2. To avoid this unphysical phenomenon near the fracture region, the cutoff parameter D_1 is set to be 2.0 Å in our simulation.[30]

The ideal unstrained infinite graphene is isotropic, but it generally loses the isotropy under stretching conditions,[31] which is sorted as the longitudinal mode (LM) and the transverse mode (TM) shown in Figure 1. The fracture strength and strain of LM are lower than those of TM, while the Young's modulus of LM is higher than that of TM. Therefore, we focus on the LM stretching of graphene in this work. The isothermal-isobaric ensemble (NPT) MD simulation is performed on the graphene with a fixed size of 12.64×11.07 nm^2, which contains $N=5400$ atoms in the defect-free state, the pressure P is fixed to be 1 bar, and the temperature T is fixed to be 300 K. The periodic boundary condition was applied to avoid the edge effect along the transverse direction.[32] At the preliminary stage of each simulation, a slow relaxation process (*i.e.*, *ca.* 200 ps) is employed to eliminate shape instabilities correlated with random velocity initialization. The non-equilibrium simulation mode is applied to allow graphene edges to move along the stretching direction at a constant strain rate. The fracture strength and strain will be slightly reduced by lowering the strain rate. Balancing the simulation efficiency and the result accuracy, the strain rate in this work is set to be 10^{-3} ps^{-1}, and the time step is 0.1 fs.

Results and Discussion

According to the Griffith's theory, the shape and size of defects, rather than the bonding strength, play a key role in the fracture strength. However, it is formidable to enumerate all sorts of vacancies. Thus, only some simple vacancy types are considered in this paper. These vacancies are simplified models for more complicated defects that exist in graphene productions and served to further the understanding of more complicated vacancies in reality. Two atom-vacancy structures are considered, as depicted in Figure 1, which are the rectangular vacancy in Figure 1a and the circular vacancy in Figure 1b. The size of the rectangular vacancy is usually defined by the number of carbon rings occupied by the edges of the rectangular vacancy (*i.e.*, edge a, and edge b). Yet the size is insufficient to define the rectangular vacancy, as different carbon-carbon bonding styles will appear even we fix the size of edge b. To be specific, the corner carbon ring on the edge b of the rectangular vacancy is defined as the first carbon ring, which is denoted by A (Figure 1a). Similarly, the second carbon ring on edge b is defined as carbon ring B or C, and the rest can be defined in the similar way. Therefore, the rectangular vacancy in Figure 1a can be

named by "a6b3AC" (including atom m and n) and "a6b3AB" (excluding atom m and n). For the circular vacancy, which only contains carbon ring A and C on the crack tip, hence the circular vacancy can be defined by the number of carbon rings along the diameter, for example, the vacancy in Figure 1b is named by "R10". In addition, the label of "bxAC" (x=2, 3, 4, ⋯) is referred to as a series of rectangular vacancies that possess the same edge b (*i.e.*, occupying A and C), but vary in the size of edge a.

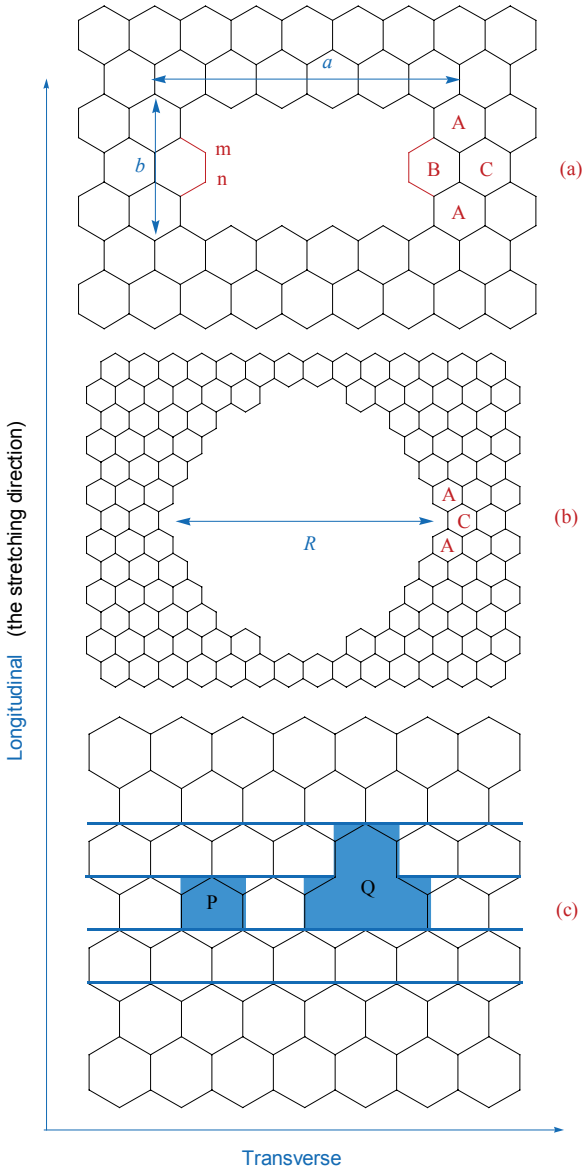

Figure 1 The definition of (a) the rectangular vacancy, (b) circular vacancy in graphene sheet, and (c) the effective spring model.

Young's modulus

We performed MD simulation for the mechanical properties of both defect-free and defected graphene. The defect-free graphene exhibits nonlinear elastic behavior, assuming its thickness to be about 3.4 Å, and then its Young's modulus E can be identified from the simulation as (1.090±0.003) TPa, the fracture strength σ_c is identified as *ca.* 90.8 GPa, the fracture strain ε_c is identified as *ca.* 0.137, and the Poisson's ratio is identified as *ca.* 0.2. All these results agree very well with previously reported work.[33]

To further explore how the Young's modulus of graphene varies with the defect shape and concentration, an effective spring model is proposed, wherein a single graphene sheet is divided into n rows, each row consists of m cells, and the size of a single cell equals to that of a single carbon ring (*i.e.*, region P in Figure 1c). Owing to the linear elastic property of graphene under small deformation, each cell can be viewed as a spring along the stretching direction, the micro-sized modulus of which is defined as E_{mic}. For the graphene with vacancy defects, assuming that the total stress exerted on each row is the same, the number of cell in a specific row x is m_x, the Young's modulus of this specific row x is $E_x = m_x E_{mic}/m$. Then the Young's modulus of the graphene with vacancy defects can be calculated by Eq. (2).

$$E = \frac{nE_{mic}}{\sum_{x=1}^{n} \frac{m}{m_x}} \tag{2}$$

For an infinitively large graphene sheet with finite defected rows, the denominator of the right part of Eq. (2) approximately equals to n, and thus $E = E_{mic}$, indicating that the Young's modulus is independent on the size of vacancy defects.

For a finite graphene sheet with rectangular vacancy, the Young's modulus can be calculated by Eq. (3).

$$E = \frac{nm'}{nm' + n'm - n'm'} E_{mic} \tag{3}$$

where $m' = m - a$ is the cell number in each defected row, n' is the number of defected row in the graphene sheet. The MD simulation reveals that the energy of carbon atoms nearby the vacancy edge a is lower than average during the stretching process, which is caused by the missing of carbon-carbon bonding between the two a edges of the vacancy. The size of the region with such lower energy is related to the size of edge a. Accordingly in the effective spring model, we assume that no stress is exerted on these carbon atoms, resulting in the increase of the effective size of edge b. Supposing that the number of the rows in the stress-free state equals to the length of edge a, then the number of defected rows n' in each graphene sheet approximately equals to $ka + b$, where k is a constant supposed to be 1.2. The Young's modulus of the graphene sheets (*i.e.*, n=60, m=45 based on our MD simulation) with various-sized rectangular vacancies can be calculated from the effective spring model (as shown in Figure 2), which are close to those derived from the MD simulation, suggesting that the Young's modulus of a finite graphene sheet with rectangular vacancy can be increased by reducing the sizes of the vacancy edge a and b. Considering that the vacancy size of edge a influences not only the cell

number in each defected row but also the total number of defected rows in the graphene sheet, the length of vacancy edge a has a greater impact on the Young's modulus than that of edge b. In the LM stretching, the edge a is perpendicular to the stretching direction, therefore we believe that the defect size in the perpendicular direction is more relevant to the Young's modulus of the graphene.

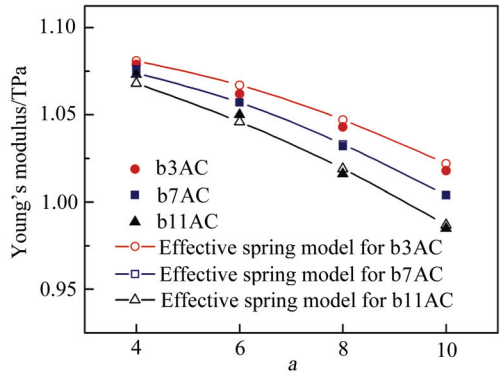

Figure 2 The Young's modulus of graphenes with various rectangular vacancy defects as a function of the size of edge a obtained from the MD simulation and the effective spring model.

In the case of isolated monatomic vacancy, each monatomic vacancy is supposed to eliminate three carbon rings nearby, as shown in the region Q of Figure 1c. The Young's modulus of the graphene sheet with varied concentrations of monatomic vacancy then can be obtained by both performing MD simulation and applying the effective spring model, and all the results are shown in Figure 3. The results derived from the MD simulation are in a good agreement with those calculated by the effective spring model. It clearly shows that the Young's modulus decreases with the increase of the vacancy concentration. The slope of the line from the effective spring model is $dE/df = -0.03$, which is nearly the same as that of -0.028 as reported in previous work using a MD simulation.[22] We can conclude that the Young's modulus shows a linear reduction by

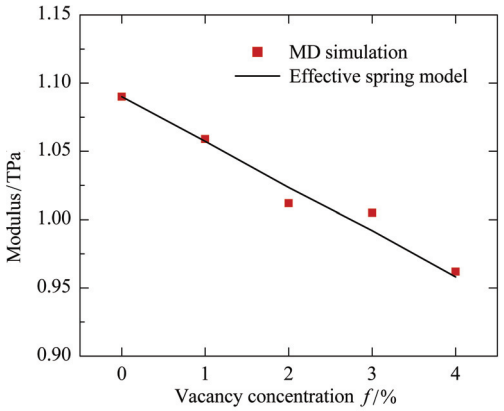

Figure 3 The Young's modulus of graphene with different monatomic-vacancy concentrations obtained from both the MD simulation and the effective spring model.

increasing the concentration of the monatomic-vacancy defects, as long as the monatomic-vacancy defects are isolated with each other when their concentrations are low.

Fracture strength and crack tip radius

Crack initiation and propagation are two crucial steps in fracture, the manner of which developed within the materials are indicative of the fracture modes. The crack initiation of graphene is accompanied by the breaking down of the carbon-carbon bonding. Once the crack is initiated, it will quickly propagate through the whole graphene sheet even without being stretched, indicating the crack propagation of graphene is a spontaneous process. According to the results of MD simulation, we found that the fracture behavior of graphene largely depends on the shape of the vacancy defects (Figure 1). For the graphene sheet with "b3AC type rectangular vacancy, the crack is initiated by breaking the carbon-carbon bonding in carbon ring C, in which there are two bonds along the stretching direction and the breakage happens on the one that connects carbon ring A (*i.e.*, the vacancy "a8b3AC" shown in Figure 4a). For the graphene sheet with "b3AB" type rectangular vacancy, the crack is initiated by breaking the carbon-carbon bonding in carbon ring B, in which there are two bonds along the stretching direction and the breakage happens on the one that in between the B and C rings (*i.e.*, the vacancy "a6b3AB" shown in Figure 4b). For the graphene sheet with "bxAC" type vacancy ($x > 3$), the crack is initiated by breaking the carbon-carbon bonding in carbon ring A, which is along the stretching

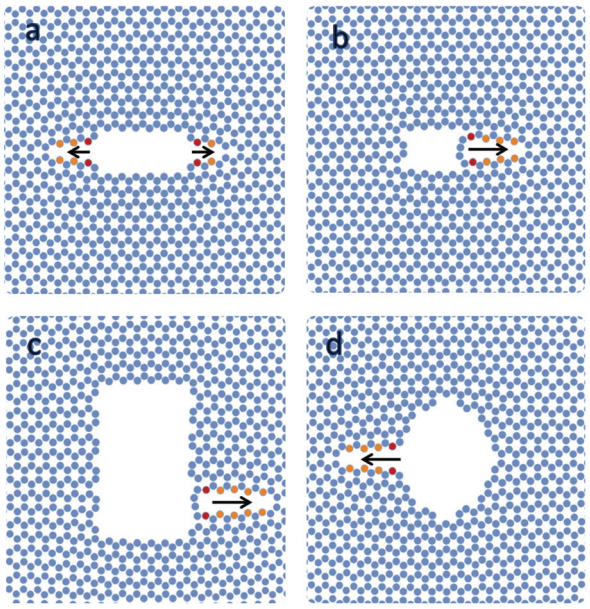

Figure 4 The crack initiation of graphene with vacancy defects of "a8b3AC" (a), "a6b3AB" (b), "a8b11AC" (c), and "R8" (d). The atoms in red were bonded incipiently, and their break as the crack initiation points. The atoms in orange were bonded incipiently, and their bonds break during crack propagation, whose orientations are represented by the arrows.

direction and is connected to the C ring (*i.e.*, the vacancy "a8b11AB" shown in Figure 4c). For the graphene sheet with circular vacancy, the crack is initiated by breaking the carbon-carbon bonding in carbon ring C, which is similar to "b3AC" type (*i.e.*, the vacancy "R8" shown in Figure 4d). For all these cases above, the cracks always propagate along the transverse direction and ultimately extend across the whole graphene sheet.

Figure 5 shows the fracture strength of graphene with various rectangular and circular vacancies. When the edge-a length of a "b3AC" type rectangular vacancy equals to the diameter of a circular vacancy, the fracture strength of the "b3AC" type rectangular vacancy is close to that of the circular vacancy, which can be ascribed to their similar crack tips and crack-initiation position. Zhao and coworkers have studied the fracture behavior of graphene with the "b3AC" type vacancy,[30] in which the crack tip radius was suggested to be $\rho = 2l_{bond}$, $l_{bond} = 1.42$ Å is the carbon-carbon bonding length. Based on QFM, the minimum fracture quantum is $L_0 = 2l\cos(\pi/3) = 2.46$ Å. The vacancy length $2l = a \times L_0 - \rho$, where a is the number of carbon ring along the vacancy edge a. The fracture strength of the graphene with "b3AC" type vacancy calculated by QFM is also shown in Figure 5, which is similar to those of MD simulation. Additionally, the fracture strength of the graphene with "a8b3AC" vacancy will reduce 4% if dangling carbon atoms are bonded on the vacancy edge a, which is attributed to the increasing stiffness of the crack edge a.

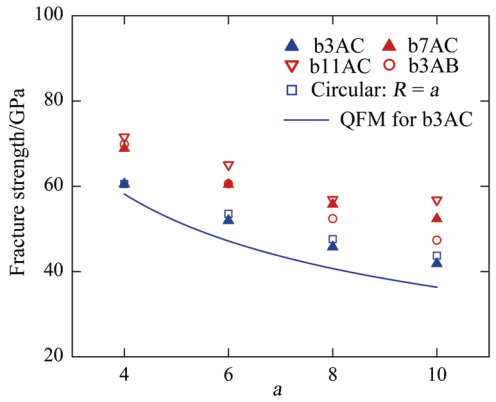

Figure 5 The fracture strength of graphene with rectangular and circular vacancies obtained from the MD simulation and the fracture strength of graphene with "a8b3AC" vacancy derived from the quantized fracture mechanics (QFM).

In general, the crack of graphene with "bxAC" (x>3) vacancy is initiated in the carbon ring A (except the ones in the corner of the rectangle), whose two carbon atoms along the side can be considered as the atoms m and n in the "b3AB" type shown in Figure 1a. Owing to the blunting effect of atoms m and n, which also contributes to reducing the stress concentration around the crack tip, the crack tip is blunted, leading to an enhanced fracture strength in the graphene with "bxAC" (x>3) vacancy, as compared to that of "b3AC" vacancy. The crack tip radiuses ρ of the "bxAC" (x>3) vacancies can be calculated from Eq. (1) as a function of the size of edge a, which are shown in Figure 6. The radiuses ρ of these "bxAC" (x>3) vacancies are nearly the same (*i.e.*, *ca.* 4.44 Å) when the size of edge a is small (*i.e.*, *ca.* 4). When the size of edge a increases, the radiuses ρ of these "bxAC" (x>3) vacancies also increase, and the vacancy with longer edge b exhibits a larger crack tip radius, indicating that both edges a and b are able to blunt the vacancy. According to previous work,[19] the vacancies with various shapes approximately exhibit two types of fracture strength when their cross sections are similar. Accordingly, the vacancies could be simply categorized as "slit like" and "blunt" by their fracture strength. The crack tip radius is about 2.84 Å for "slit like" vacancies, and 4.44 Å for "blunt" vacancies, when the lengths of their cross sections are short (*i.e.*, the length of edge a below 4). The blunting effect is usually ascribed to the atoms m and n, which contribute to releasing the stress concentration by bearing the stress at the crack tip. For the vacancy with a long edge a (*i.e.*, the length of edge a above 4), the crack tip radius increases as a function of the length of edge a, which may result from the blunting effect brought by the edges a and b. The deflection of edge a would reduce the stress concentration along the edge. Moreover, the longer the edge b is, the more effective the reduction is, as shown in Figure 6.

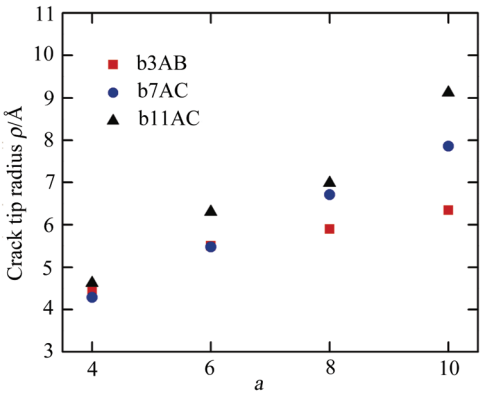

Figure 6 The crack tip radius of various rectangular vacancies calculated via QFM based on the results from MD simulations.

Conclusions

In conclusion, we have investigated the Young's modulus and the fracture strength of graphene with various vacancy defects using the MD simulation, the effective spring model, and the quantized fracture mechanics. By comparing the results of the MD simulation and the quantized fracture mechanics, we found that the Young's modulus of graphene is largely related to the size of vacancy defect perpendicular to the stretching direction. In the case of isolated monatomic-vacancy defect, the Young's modulus of graphene mainly depends on the concentration of the vacancy defects, and a

linear reduction of the modulus with the increased concentrations of the monatomic vacancy by the slope of −0.03 is obtained. For the study of fracture strength of graphene with different vacancy defects, different crack initiation behaviors are revealed, and it is demonstrated that the blunting effect of vacancy edges plays an important role in the fracture crack initiation and propagation of graphene. The characterized crack tip radius of 4.44 Å is observed, which can be used to estimate the fracture strength due to "blunt" vacancy defects.

Acknowledgement

We gratefully acknowledge the financial support from the National Basic Research Program of China (No. 2011CB605700).

References

[1] Novoselov, K. S.; Geim, A. K.; Morozov, S. V.; Jiang, D.; Katsnelson, M. I.; Grigorieva, I. V.; Dubonos, S. V.; Firsov, A. A. *Nature* **2005**, *438*, 197.
[2] Castro Neto, A. H.; Guinea, F.; Peres, N. M. R.; Novoselov, K. S.; Geim, A. K. *Rev. Mod. Phys*. **2009**, *81*, 109.
[3] Zhang, Y. B.; Tan, Y. W.; Stormer, H. L.; Kim, P. *Nature* **2005**, *438*, 201.
[4] Stankovich, S.; Dikin, D. A.; Dommett, G. H. B.; Kohlhaas, K. M.; Zimney, E. J.; Stach, E. A.; Piner, R. D.; Nguyen, S. T.; Ruoff, R. S. *Nature* **2006**, *442*, 282.
[5] Balandin, A. A.; Ghosh, S.; Bao, W.; Calizo, I.; Teweldebrhan, D.; Miao, F.; Lau, C. N. *Nano Lett*. **2008**, *8*, 902.
[6] Lee, C.; Wei, X.; Kysar, J. W.; Hone, J. *Science* **2008**, *321*, 385.
[7] Rao, C. N. R.; Sood, A. K.; Subrahmanyam, K. S.; Govindaraj, A. *Angew. Chem.*, *Int. Ed.* **2009**, *48*, 7752.
[8] Rummeli, M. H.; Rocha, C. G.; Ortmann, F.; Ibrahim, I.; Sevincli, H.; Borrnert, F.; Kunstmann, J.; Bachmatiuk, A.; Potschke, M.; Shiraishi, M.; Meyyappan, M.; Buchner, B.; Roche, S.; Cuniberti, G. *Adv. Mater.* **2011**, *23*, 4471.
[9] Novoselov, K. S.; Geim, A. K.; Morozov, S. V.; Jiang, D.; Zhang, Y.; Dubonos, S. V.; Grigorieva, I. V.; Firsov, A. A. *Science* **2004**, *306*, 666.
[10] Geim, A. K.; Novoselov, K. S. *Nat. Mater.* **2007**, *6*, 183.
[11] Park, S.; Ruoff, R. S. *Nat. Nanotechnol.* **2009**, *4*, 217.
[12] Allen, M. J.; Tung, V. C.; Kaner, R. B. *Chem. Rev.* **2010**, *110*, 132.
[13] Banhart, F.; Kotakoski, J.; Krasheninnikov, A. V. *ACS Nano* **2011**, *5*, 26.
[14] Wang, J. C.; Wang, X. B.; Wan, L.; Yang, Y. K.; Wang, S. M. *Chin. J. Chem.* **2010**, *28*, 1935.
[15] Gass, M. H.; Bangert, U.; Bleloch, A. L.; Wang, P.; Nair, R. R.; Geim, A. K. *Nat. Nanotechnol*. **2008**, *3*, 676.
[16] Huang, P. Y.; Ruiz-Vargas, C. S.; van der Zande, A. M.; Whitney, W. S.; Levendorf, M. P.; Kevek, J. W.; Garg, S.; Alden, J. S.; Hustedt, C. J.; Zhu, Y.; Park, J.; McEuen, P. L.; Muller, D. A. *Nature* **2011**, *469*, 389.
[17] Ruiz-Vargas, C. S.; Zhuang, H. L.; Huang, P. Y.; van der Zande, A. M.; Garg, S.; McEuen, P. L.; Muller, D. A.; Hennig, R. G.; Park, J. *Nano Lett.* **2011**, *11*, 2259.
[18] Kotakoski, J.; Meyer, J. C. *Phys. Rev. B* **2012**, *85*, 195447.
[19] Khare, R.; Mielke, S. L.; Paci, J. T.; Zhang, S.; Ballarini, R.; Schatz, G. C.; Belytschko, T. *Phys. Rev. B* **2007**, *75*, 5412.
[20] Xiao, J. R.; Staniszewski, J.; Gillespie Jr, J. W. *Compos. Struct*. **2009**, *88*, 602.
[21] Nardelli, M. B.; Yakobson, B. I.; Bernholc, J. *Phys. Rev. B* **1998**, *57*, 4277.
[22] Hao, F.; Fang, D.; Xu, Z. *Appl. Phys. Lett.* **2011**, *99*, 041901.
[23] Tapia, A.; Peon-Escalante, R.; Villanueva, C.; Aviles, F. *Comp. Mater. Sci.* **2012**, *55*, 255.
[24] Tserpes, K. I.; Papanikos, P. *Compos. Part B-Eng.* **2005**, *36*, 468.
[25] Pugno, N. M.; Ruoff, R. S. *Philos. Mag.* **2004**, *84*, 2829.
[26] Plimpton, S. J. *Comput. Phys.* **1995**, *117*, 1.
[27] Tersoff, J. *Phys. Rev. B* **1988**, *37*, 6991.
[28] Brenner, D. W. *Phys. Rev. B* **1992**, *46*, 1948.
[29] Tsai, P. C.; Jeng, Y. R.; Fang, T. H. *Phys. Rev. B* **2006**, *74*, 5406.
[30] Zhao, H.; Aluru, N. R. *J. Appl. Phys.* **2010**, *108*, 64321.
[31] Baimova, Y. A.; Dmitriev, S. V.; Savin, A. V.; Kivshar, Y. S. *Phys. Solid State* **2012**, *54*, 866.
[32] Lu, Q.; Gao, W.; Huang, R. *Model. Simul. Mater. Sci. Eng.* **2011**, *19*, 54006.
[33] Zhao, H.; Min, K.; Aluru, N. R. *Nano Lett.* **2009**, *9*, 3012.

(Cheng, F.)

